Ferroelectricity

DOI: 10.1002/anie.201302188

Ferroelectricity Driven by Twisting of Silicate Tetrahedral Chains**

Hiroki Taniguchi, Akihide Kuwabara, Jungeun Kim, Younghun Kim, Hiroki Moriwake, Sungwng Kim, Takuya Hoshiyama, Tsukasa Koyama, Shigeo Mori, Masaki Takata, Hideo Hosono, Yoshiyuki Inaguma, and Mitsuru Itoh*

Because of its diverse functionality, ferroelectricity plays a key role in electronic and optical technologies.[1] Ferroelectric materials are characterized by a switchable polarization caused by spontaneous displacements of cations relative to anions, which occurs in centrosymmetric to noncentrosymmetric ferroelectric phase transitions. In the case of displacive-type phase transitions, the phase transition is driven by the freezing of a zone-center optical phonon mode, "soft mode", using an eigenvector similar to the polar displacement observed in the ferroelectric phase.[2] Recent studies have clarified that the soft mode instability in conventional perovskite-type oxides is caused by covalency between the cations and oxygen ions in the octahedral oxygen units.[3] Current ferroelectric applications rely heavily upon toxic Pb-based compounds, because the strong covalency of Pb–O causes structural instability in these compounds and induces the large spontaneous polarization. Alternately, Bi-based perovskite-type oxides like $BiFeO_3$ (BFO), have recently attracted attention because of their high Curie temperature (T_c) and its large polarization that is comparable to the Pb-based ferroelectrics.[4] The 6s 1orbital of Bi hybridizes with the adjacent oxygen 2p orbital to induce the large polar displacement of Bi.[5] Also in this case, the ferroelectricity stems from the unique property of the specific element, Bi. Such a strong element dependence of ferroelectric oxides demands new principle guidelines for designing ferroelectric materials.[6]

Here, we report for the first time the ferroelectric phase transition driven by the structural instability of pyroxenoid-type one-dimensional chains of oxygen tetrahedra, which occur in the silicate-based compound Bi_2SiO_5 (BSO). BSO has a layered structure, which comprises a single layer of one-dimensional silicate chains sandwiched between Bi_2O_2 sheets (Figure 1A). The ferroelectric phase transition at 663 K is induced by the freezing of the soft mode that stems from the twisting of silicate chains. The ferroelectricity is verified by a direct observation of the P–E hysteresis loops and arises from the structural instability of the tetrahedral oxygen chains. Therefore, the present finding offers a new route for designing environmentally friendly ferroelectric oxides that are free from specific element constraints.

The crystal structure of BSO has previously been reported to be an orthorhombic $Cmc2_1$ at room temperature.[7] Our transmission electron microscopy (TEM) observations, however, reveal that the crystallographic β angle of BSO slightly deviates from 90° at room temperature, indicating a monoclinic distortion of BSO (see Figure S1A in the Supporting Information). X-ray powder diffraction analysis indicates that BSO has a monoclinic Cc crystal structure with lattice parameters of $a = 15.1193(1)$ Å, $b = 5.4435(1)$ Å, $c = 5.2892(1)$ Å, and $\beta = 90.0695(20)°$ (Figure S2A). At 793 K, the β angle changes to 90°, demonstrating a structural phase transition from the monoclinic to orthorhombic phase (Figure S1B). The high-temperature orthorhombic phase was

---

[*] Prof. H. Taniguchi,[+] Prof. H. Hosono, Prof. M. Itoh
Materials and Structures Laboratory
Tokyo Institute of Technology
Yokohama 226-8503 (Japan)
E-mail: hiroki_taniguchi@cc.nagoya-u.ac.jp

Dr. A. Kuwabara, Dr. H. Moriwake
Nanostructures Research Laboratory (Japan) Fine Ceramics Center
Nagoya 456-8587 (Japan)

Dr. J. Kim, Prof. M. Takata
Japan Synchrotron Radiation Research Institute
Sayo-gun, Hyogo 679-5198 (Japan)

Y. Kim, Prof. M. Takata
Graduate School of Frontier Sciences
The University of Tokyo
Kashiwa, Chiba 277-8561 (Japan)

Prof. S. Kim
Department of Energy Science, Sungkyunkwan University
Jangan-Gu, Suwon 440-746 (Korea)

T. Hoshiyama, T. Koyama, Prof. S. Mori
Department of Materials Science
Osaka Prefecture University
Sakai, Osaka 599-8531 (Japan)

Prof. M. Takata
RIKEN Harima Institute
Sayo-gun, Hyogo 679-5148 (Japan)

Prof. H. Hosono
Frontier Research Center, Tokyo Institute of Technology
Yokohama 226-8503 (Japan)

Prof. Y. Inaguma
Faculty of Science, Gakushuin University
Toshima-ku, Tokyo 171-8588 (Japan)

[+] Current address:
Department of Physics, Nagoya University
Furo-cho, Chikusa, Nagoya 464-8602 (Japan)

[**] This work was supported by the Ministry of Education, Culture, Sports, Science, and Technology of Japan through a Grant-in-Aid for Young Scientists (B, grant number 24760543) and Scientific Research (C, grant number 24560833), Hitachi Metals—Materials Science Foundation, and MEXT Element Strategy Initiative Project.

Supporting information for this article is available on the WWW under http://dx.doi.org/10.1002/anie.201302188.

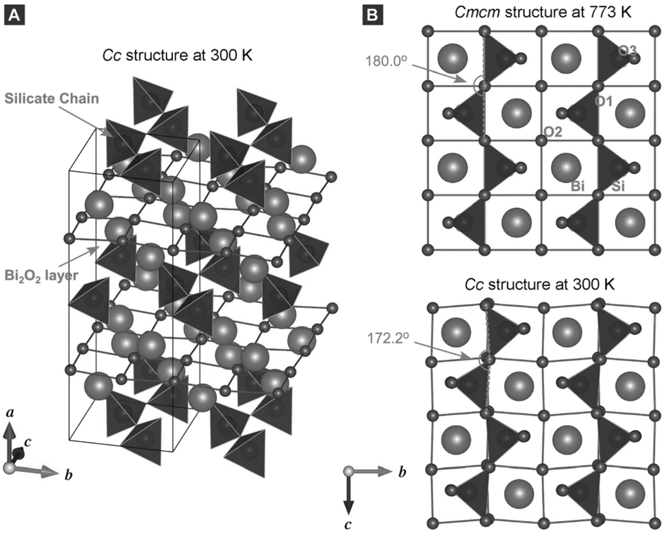

Figure 1. A) The crystal structure of BSO in the ferroelectric phase. The one-dimensional chains of the SiO_4 tetrahedra running along the *c* axis are sandwiched by Bi_2O_2 layers. The cleavage plane is normal to the *a* axis. B) The crystal structures of BSO projected onto the *b*–*c* plane. The upper and lower figures show the high-temperature (*Cmcm*) and low-temperature (*Cc*) structures, respectively. The ···O1-O1-O1··· chain is twisted by 172.2° in the *Cc* phase, which is in contrast to the linear configuration shown in the *Cmcm* phase.

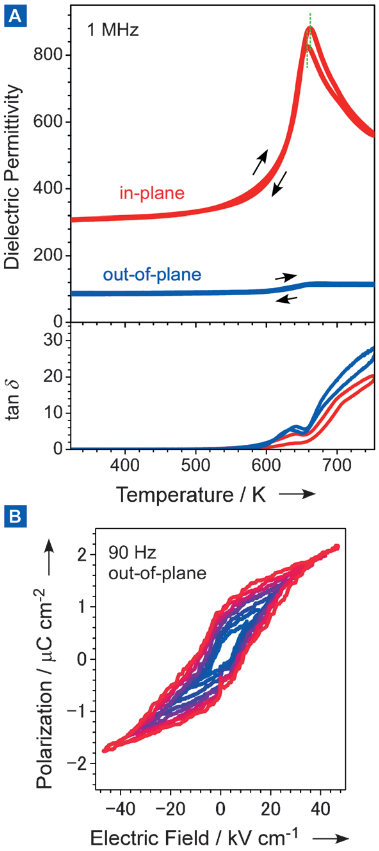

Figure 2. A) The temperature dependence of the dielectric permittivity and tanδ of the oriented polycrystalline BSO at 1 MHz measured along the in-plane (red curves) and the out-of-plane directions, respectively. The red and blue arrows denote the heating and subsequent cooling processes, respectively. The culminated temperatures for the heating and cooling processes of the in-plane measurement are indicated by broken lines. B) *P*–*E* hysteresis loop of BSO at 573 K, which was measured using a Sawyer–Tower circuit.

also investigated by X-ray powder diffraction at 773 K. Based on Rietveld analyses, it was established that BSO has an orthorhombic *Cmcm* structure with lattice parameters of $a = 15.1968(1)$ Å, $b = 5.4843(1)$ Å, and $c = 5.2964(1)$ Å (Figure S2 B). In the high-temperature phase of BSO (Figure 1 B), the ···O1-O1-O1··· bonds that form the one-dimensional chains of the SiO_4 tetrahedral units are linear. As the temperature decreases, the bonds twist with an angle of 172.2°, which is accompanied by a coherent displacement of the Bi ions, and a distortion of the O3 grid patterns. The spontaneous polarization along the *c* direction in the low-temperature phase is induced by the relative displacement of the anionic SiO_4 tetrahedral units and cationic Bi_2O_2 layers. Concurrently, the Bi ions slightly shift to a direction normal to the O3 grids, thereby inducing the polarization along the *a* direction.

Figure 2 A presents the temperature dependences of the dielectric permittivity and the dielectric loss (tanδ) in polycrystalline BSO. Since the BSO is obtained as a very thin crystal with a wide (100) cleavage plane, which includes 90° twinning of the (010) and (001) planes, the dielectric measurements (1 MHz) were performed in the oriented polycrystalline BSO for the out-of-plane direction along the *a* axis and the in-plane direction along the *b* and *c* axes (red and blue lines in Figure 2 A, respectively). The dielectric permittivity for the in-plane direction gradually increases with temperature and culminates at 663 K, indicating the onset of the ferroelectric phase transition. A subsequent cooling process shows a small hysteresis in the peak (dotted lines in Figure 2 A), which indicates a weak first-order phase transition. The dielectric permittivity in the out-of-plane direction only shows a small kink, indicating that the critical polar fluctuation lies in the (100) plane. An increasing tanδ observed in the high-temperature region stems from ionic conduction. The polarization switching is demonstrated in the single crystal of BSO along the *a* direction, at an applied voltage of ±10 to ±45 kV cm^{-1}. As seen in Figure 2 B, a well-saturated *P*–*E* hysteresis loop is observed at 573 K, confirming the occurrence of ferroelectricity in BSO. The present result indicates that the spontaneous polarization projected onto the *a* direction, P_s^a, is 0.8 μC cm^{-2}. The small out-of-plane polarization agrees well with the slight monoclinic distortion of BSO in the ferroelectric phase.

Figure 3 A shows low-frequency Raman spectra of BSO from 83.15 to 723.15 K. As indicated by the red arrow in the figure, the low-frequency peak observed around 70 cm^{-1} at 83.15 K, decreases to zero frequency with increasing temperature. The peak completely vanishes on further heating, confirming the polar character of this mode (the polar mode is Raman-inactive in the centrosymmetric *Cmcm* phase). This is the ferroelectric soft mode in BSO. In displacive-type ferroelectric phase transitions, the soft mode softens by obeying Cochran's law, $\omega_{\text{soft}} = C\,|\,T - T_c\,|^{0.5} + \Delta\omega$, where ω_{soft}, C, T_c, and $\Delta\omega$ are the soft-mode frequency, the Curie constant, the Curie

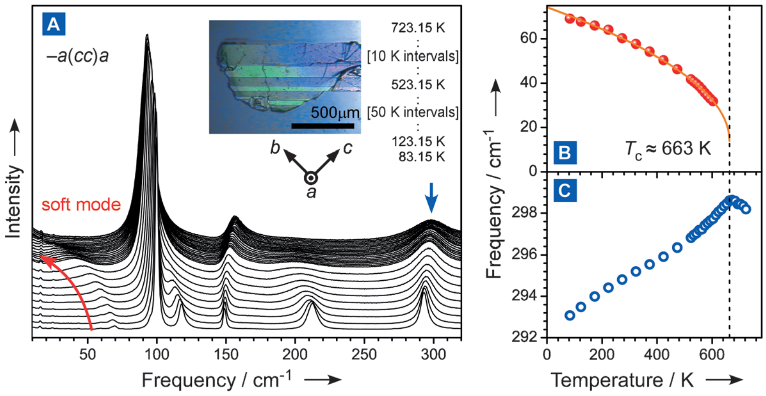

Figure 3. A) The temperature dependence (83.15 to 723.15 K) of the Raman spectrum of BSO. The inset shows the single-crystal plate of BSO with the crystallographic axes. B) The temperature dependence of the soft-mode frequency, which was analyzed by a spectral fitting using the damped harmonic oscillator (DHO) model, $I(\omega) = A(\omega_0^2\Gamma\omega/((\omega_0^2-\omega^2)^2+\Gamma^2\omega^2))$, where A, ω_0, and Γ denote the amplitude, the harmonic frequency, and the damping factor of the oscillation, respectively. The soft-mode frequency ω_s is calculated by $(\omega_0^2-\Gamma^2)^{1/2}$ according to Ref. [8]. The curve shown in panel B is calculated using Cochran's law. C) The temperature dependence of the frequency for the peak around 300 cm^{-1}, which was obtained by a spectral fitting using the DHO model.

temperature, and the frequency offset for the first-order phase transition, respectively.[2a,b] Figure 3B shows a temperature dependence of ω_{soft}. The data points close to 663 K are omitted because of an uncertainty in the analyses because of overdamping of the soft mode. To obtain the exact T_c that is estimated from the Raman spectra, we examined the temperature dependence of the 300 cm^{-1} peak (blue arrow in Figure 3A). The temperature dependence of the peak position presented in Figure 3C shows a distinct cusp around 663 K, corresponding to T_c. The T_c value agrees with the anomaly in the dielectric permittivity shown in Figure 2A. The temperature dependence of the soft-mode frequency was examined using Cochran's law at $T_c = 663$ K, leading to a good fit with the parameters of $C = 2.3$ and $\Delta\omega = 13.9$ cm^{-1} (solid line in Figure 3B). This result confirms the displacive-type ferroelectric phase transition of BSO, which is driven by the ferroelectric soft mode.

Phonon dispersion curves in the high-temperature *Cmcm* phase obtained by first principles calculations are shown in the left panel of Figure 4A. The ferroelectric soft mode is characterized by the Γ-point imaginary frequency in the paraelectric phase, which results from the vibrational instability in the centrosymmetric structure.[9] The calculation clarifies the existence of the soft mode in the *Cmcm* phase, as indicated by the arrows. A discontinuity in the soft mode dispersion toward the Z-point is caused by the splitting of the longitudinal and transverse components, indicating that the soft mode polarizes along the *c*-direction. In the *Cc* phase phonon dispersion curves, however, the soft mode vanishes, confirming the *Cc* crystal symmetry for the ferroelectric ground state of BSO. The displacement pattern of the soft mode is presented in Figure 4B with the equilibrium structure of the *Cmcm* phase (see Figure S3). The equilibrium paraelectric structure in the central panel, obtained by first-principles calculations, is consistent with that determined by X-ray powder diffraction, as shown in Figure 1B. The displacement pattern in the (100) plane is composed of twisted silicate tetrahedral chains, which are accompanied by the deformation of the oxygen grid pattern. Concurrently the Bi ions show a slight shift along the *c* axis. At temperatures sufficiently higher than T_c, the silicate tetrahedral chains alternate between opposing twist configurations. As the temperature approaches T_c, the frequency decreases toward zero and polarization is induced in BSO when it freezes at T_c. The net polarization is generated cooperatively with the concomitant distortions of the Bi_2O_2 sublattice. The freezing of the calculated soft mode displacement reduces the symmetry as the *Cmcm* structure changes to *Cmc*2$_1$. A small monoclinic distortion occurs at T_c, as the total energy of *Cc* is less than that of *Cmc*2$_1$; the difference, estimated from first-principles calculations is 0.2 meV/Bi_2SiO_5. In addition to the Γ-point, several unstable modes are observed at the Y- and S-points. According to the calculation, the Γ-point distortion is the energetically most favor-

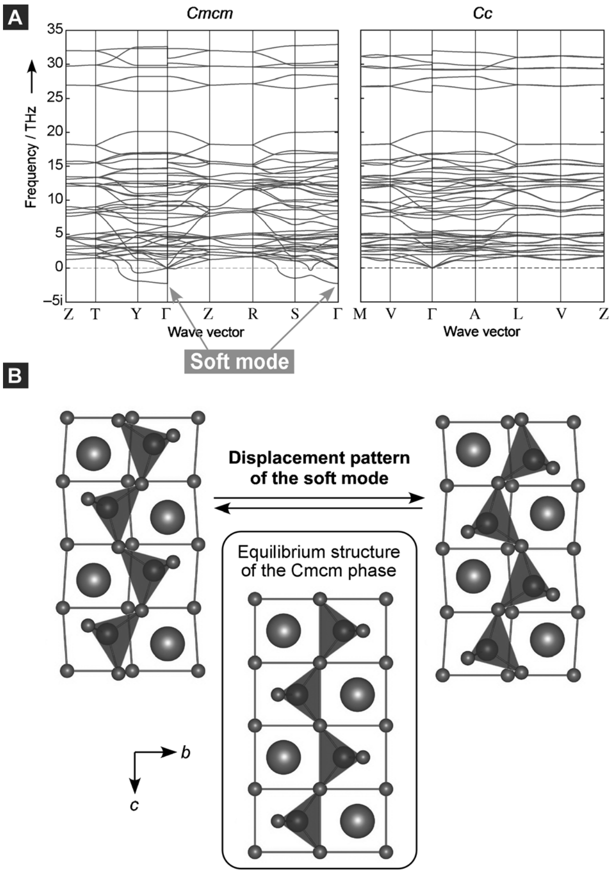

Figure 4. A) Phonon dispersion curves of BSO for the paraelectric *Cmcm* (left) and *Cc* (right) phases. Arrows indicate the ferroelectric soft mode at the *Γ*-point of the Brillouin zone. B) The displacement pattern for the ferroelectric soft mode. The central illustration presents the *Cmcm* phase equilibrium structure of BSO. The illustrations are projected onto the *b*–*c* plane with selected ions for simplicity.

able among all corresponding unstable mode distortions (Table S2). The thin crystal shape allows only polarization measurements along the *a* axis (Figure 2B), therefore the in-plane polarization along the *c* axis was not obtained experimentally and was estimated from the Berry phase calculation of the optimized *Cc* structure. The calculated P_s^c value of about 14.5 $\mu C\,cm^{-2}$ along the *c* direction indicates the potential of the tetrahedral chain for achieving robust ferroelectricity. The calculated out-of-plane polarization is 0.1 $\mu C\,cm^{-2}$, which is roughly consistent with the experimental value. The calculated structural parameters, Born effective charges, and dielectric permittivity tensors are given in the Tables S3, S4, and S5. The ratios of lattice constants agree well with the experimental results, although the individual values are slightly underestimated by approximately 2%.

The twisting of silicate chains, which mainly compose the soft mode displacements in BSO, are also found in silicates, such as cristobalite, the high-temperature form of quartz. Cristobalite is composed only of parallel connected silicate chains. Interestingly, the α–β transition of cristobalite is driven by the twisting of the silicate chain, similar to BSO.[10] This suggests that the silicate chains themselves possess unstable twisting fluctuations to induce structural phase transitions. Thus, we believe that the ferroelectric phase transition of BSO stems intrinsically from the structural instability of the silicate chains, even though the distortion of the Bi_2O_2 sublattice also takes part in the ferroelectric soft mode displacement. This is distinct from traditional ferroelectric materials, where the ferroelectricity is designed by the arrangement of the octahedral oxygen units and interstitial cations. The present result sheds light on a development of "engineering of tetrahedra" for the ferroelectrics, beyond the conventional "engineering of octahedra". The one-dimensional tetrahedral chains can be found in many ubiquitous oxides, such as framework silicates and aluminates, which are abundant in the earth's crust.[11] We therefore believe that the present findings will also help provide new guidelines for the development of environmentally friendly ferroelectric oxides.

Experimental Section

We crystallized BSO single crystals from a melt: Bi_2O_3 and SiO_2 powders with a 1:1 molar ratio were mixed together in an agate mortar, and heated in a Pt crucible at 1373 K over a period of 2 h. The resulting melt was subsequently cooled at a rate of 10 $K\,h^{-1}$ to 1073 K, followed by furnace cooling to room temperature. We obtained BSO thin plates with (100) cleavage planes (the inset of Figure 3A). Twin structures of several hundred microns are observed in the polarized microscope images. We also fabricated BSO ceramics by Spark plasma sintering (SPS) for the BSO powder, which was prepared by grinding the single crystals.

The micro-Raman scattering experiments were performed with an Ar^+ laser (514.5 nm) at approximately 10 mW, which was focused onto the BSO single crystal using a 50× objective lens (numerical aperture, N.A. = 0.55) to select a single domain area. The scattered light was collected with a back scattering geometry and analyzed using a polarizer, where a scattering configuration was *-a*(*cc*)*a* according to Porto's notation (see Figure 3A). Raman spectra were obtained using a Horiba-Jovin-Yvon T64000 Raman spectrometer equipped with a liquid N_2-cooled charge-coupled device (CCD) camera. The temperature of the sample was controlled using a Linkam Scientific Instruments THMS600 microscope stage with an accuracy of ± 0.1 K.

First-principles calculations were performed using the projector augmented wave method and the local density approximation (LDA) implemented in the VASP code.[12] Plane waves up to 500 eV were used as basis sets. Valence electron configurations of the potentials were taken as $5d^{10}\,6s^2\,6p^3$ for Bi, $3s^2\,3p^2$ for Si, and $2s^2\,2p^4$ for O.

Primitive cells of Bi_2SiO_5 high-temperature (*Cmcm*) and low-temperature (*Cc*) phases were optimized with 5 × 5 × 5 *k*-point sampling meshes based on the Monkhorst–Pack scheme.[13] Crystal structures were fully relaxed until residual forces were less than 0.0002 $eV\,Å^{-1}$. Phonon calculations were performed using the PHONOPY code.[14] Interatomic force constants in real space were obtained from 4 × 4 × 1 supercells of conventional unit cells. In the supercell calculations, a *k*-point at (1/4 1/4 1/4) was chosen for Brillouin zone sampling. Nonequivalent atomic displacements of 0.01 Å were employed for calculations of the force constants based on symmetry analyses. A nonanalytical term correction was added to dynamical matrices to include the longitudinal optical–transverse optical (LO-TO) splitting near the Γ-point.[15] Born effective charges and dielectric constants were obtained using the linear response approach.[16] Macroscopic polarization was obtained using Berry phase calculations.[17]

X-ray powder diffraction measurements on the powder samples of Bi_2SiO_5 were carried out at the powder diffraction beamline BL02B2 (proposal number 2011B2089) of SPring-8 to obtain a high angular resolution pattern ($d < 0.5$ Å). The diffraction patterns were collected on an imaging plate installed on a large Debye–Scherrer camera.[18] The structural parameters of the room-temperature ferroelectric phase and the high-temperature phase Bi_2SiO_5 are summarized in Table S1.

Transmission electron microscopy (TEM) experiments were carried out using a JEM-2010 transmission electron microscope with an accelerating voltage of 200 kV. The reflection spots in the ED patterns (Figure S1) are indexed on the basis of the high-temperature (*Cmcm*) structure.

All crystal structures were produced using the visualization program VESTA.[19]

Received: March 15, 2013
Published online: June 14, 2013

Keywords: ferroelectricity · ferroelectric phase transition · functional oxides · oxygen tetrahedra · silicates

---

[1] G. H. Haertling, *J. Am. Ceram. Soc.* **1999**, *82*, 797–818.
[2] a) W. Cochran, *Adv. Phys.* **1960**, *9*, 387; b) W. Cochran, *Adv. Phys.* **1961**, *10*, 401; c) J. F. Scott, *Rev. Mod. Phys.* **1974**, *46*, 83.
[3] a) R. E. Cohen, *Nature* **1992**, *358*, 136–138; b) Y. Kuroiwa, S. Aoyagi, A. Sawada, J. Harada, E. Nishibori, M. Takata, M. Sakata, *Phys. Rev. Lett.* **2001**, *87*, 217601; c) H. Taniguchi, H. P. Soon, T. Shimizu, H. Moriwake, Y. J. Shan, M. Itoh, *Phys. Rev. B* **2001**, *84*, 174106.
[4] M. R. Dolgos, U. Adem, A. Manjon-Sanz, X. Wan, T. P. Comyn, T. Stevenson, J. Bennett, A. J. Bell, T. T. Tran, P. S. Halasyamani, J. B. Claridge, M. J. Rosseinsky, *Angew. Chem.* **2012**, *124*, 10928; *Angew. Chem. Int. Ed.* **2012**, *51*, 10770.
[5] a) R. Seshadri, N. A. Hill, *Chem. Mater.* **2001**, *13*, 2892–2899; b) J. B. Neaton, C. Ederer, U. V. Waghmare, N. A. Spaldin, K. M. Rabe, *Phys. Rev. B* **2005**, *71*, 014113.
[6] a) Y. Saito, H. Takao, T. Tani, T. Nonoyama, K. Takatori, T. Homma, T. Nagaya, M. Nakamura, *Nature* **2004**, *432*, 84–87; b) P. K. Panda, *J. Mater. Sci.* **2009**, *44*, 5049–5062.
[7] J. Ketterer, V. Krämer, *N. Jb. Miner. Mh.* **1986**, *H.1*, 13–18.
[8] H. Taniguchi, Y. J. Shan, H. Mori, M. Itoh, *Phys. Rev. B* **2007**, *76*, 212103.

[9] R. E. Cohen, H. Krakauer, *Phys. Rev. B* **1990**, *42*, 6416–6423.

[10] D. M. Hatch, S. Ghose, *Chem. Minerals* **1991**, *17*, 554.

[11] F. Liebau, *Structural chemistry of silicates: structure, bonding, and classification 1–6*, Springer, Berlin, **1985**.

[12] a) G. Kresse, D. Joubert, *Phys. Rev. B* **1998**, *59*, 1758–1775; b) D. M. Ceperley, B. J. Alder, *Phys. Rev. Lett.* **1980**, *45*, 566–569; c) G. Kresse, J. Furthmüller, *Phys. Rev. B* **1996**, *54*, 11169–11186.

[13] H. J. Monkhorst, J. D. Pack, *Phys. Rev. B* **1976**, *13*, 5188.

[14] a) K. Parlinski, Z. Q. Li, Y. Kawazoe, *Phys. Rev. Lett.* **1997**, *78*, 4063; b) A. Togo, F. Oba, I. Tanaka, *Phys. Rev. B* **2008**, *78*, 134106.

[15] a) X. Gonze, C. Lee, *Phys. Rev. B* **1997**, *55*, 10355; b) Y. Wang, J. J. Wang, W. Y. Wang, Z. G. Mei, S. L. Shang, L. Q. Chen, Z. K. Liu, *J. Phys. Condens. Matter* **2010**, *22*, 202201.

[16] M. Gajdoš, K. Hummer, G. Kresse, J. Furthmüller, F. Bechstedt, *Phys. Rev. B* **2006**, *73*, 045112.

[17] R. D. King-Smith, D. Vanderbilt, *Phys. Rev. B* **1993**, *47*, 1651–1654; D. Vanderbilt, R. D. King-Smith, *Phys. Rev. B* **1993**, *48*, 4442–4455.

[18] E. Nishibori, M. Takata, K. Kato, M. Sakata, Y. Kubota, S. Aoyagi, Y. Kuroiwa, M. Yamakata, N. Ikeda, *Nucl. Instrum. Methods Phys. Res. Sect. A* **2001**, *467–468*, 1045–1048.

[19] K. Momma, F. Izumi, *J. Appl. Crystallogr.* **2011**, *44*, 1272.